HELDA
HELSINGIN YLIOPISTO
HELSINGFORS UNIVERSITET
UNIVERSITY OF HELSINKI

UNIVERSITY OF HELSINKI

**https://helda.helsinki.fi**

# Synchronizing gas injections and time-resolved data acquisition for perturbation-enhanced APXPS experiments

Redekop, Evgeniy A.

2021-04-01

Redekop , E A , Johansson , N , Kokkonen , E , Urpelainen , S , da Silva , F L , Kaipio , M , Nieminen , H-E , Rehman , F , Miikkulainen , V , Ritala , M & Olsbye , U 2021 , ' Synchronizing gas injections and time-resolved data acquisition for perturbation-enhanced APXPS experiments ' , Review of Scientific Instruments , vol. 92 , no. 4 , 044101 . https://doi.org/10.1063/5.0039957

http://hdl.handle.net/10138/342264
https://doi.org/10.1063/5.0039957

unspecified
publishedVersion

*Downloaded from Helda, University of Helsinki institutional repository.*

*This is an electronic reprint of the original article.*

*This reprint may differ from the original in pagination and typographic detail.*

*Please cite the original version.*

Review of Scientific Instruments

# Synchronizing gas injections and time-resolved data acquisition for perturbation-enhanced APXPS experiments

Cite as: Rev. Sci. Instrum. **92**, 044101 (2021); https://doi.org/10.1063/5.0039957
Submitted: 08 December 2020 . Accepted: 15 March 2021 . Published Online: 01 April 2021

Evgeniy A. Redekop, Niclas Johansson, Esko Kokkonen, Samuli Urpelainen, Felipe Lopes da Silva, Mikko Kaipio, Heta-Elisa Nieminen, Foqia Rehman, Ville Miikkulainen, Mikko Ritala, and Unni Olsbye

View Online Export Citation CrossMark

ARTICLES YOU MAY BE INTERESTED IN

Understanding chemical and physical mechanisms in atomic layer deposition
The Journal of Chemical Physics **152**, 040902 (2020); https://doi.org/10.1063/1.5133390

Atomic layer deposition of AlN using atomic layer annealing–Towards high-quality AlN on vertical sidewalls
Journal of Vacuum Science & Technology A **39**, 032403 (2021); https://doi.org/10.1116/6.0000724

Simple, reversible gradient Seebeck coefficient measurement system for 300–600#K with COMSOL simulations
Review of Scientific Instruments **92**, 044903 (2021); https://doi.org/10.1063/1.5124459

MCL MAD CITY LABS INC. www.madcitylabs.com
Nanopositioning Systems
Modular Motion Control
AFM and NSOM Instruments
Single Molecule Microscopes

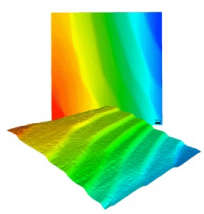
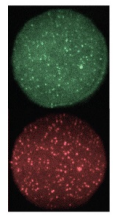



© 2021 Author(s).

AIP Publishing

Review of Scientific Instruments ARTICLE scitation.org/journal/rsi

# Synchronizing gas injections and time-resolved data acquisition for perturbation-enhanced APXPS experiments

Cite as: Rev. Sci. Instrum. 92, 044101 (2021); doi: 10.1063/5.0039957
Submitted: 8 December 2020 • Accepted: 15 March 2021 •
Published Online: 1 April 2021

View Online Export Citation CrossMark

Evgeniy A. Redekop,[1,a)] Niclas Johansson,[2] Esko Kokkonen,[2] Samuli Urpelainen,[3] Felipe Lopes da Silva,[2,3,4,5] Mikko Kaipio,[6] Heta-Elisa Nieminen,[6] Foqia Rehman,[5] Ville Miikkulainen,[6,b)] Mikko Ritala,[6] and Unni Olsbye[1]

## AFFILIATIONS

[1] Department of Chemistry, Centre for Materials Science and Nanotechnology (SMN), University of Oslo, Oslo 0371, Norway
[2] MAX IV Laboratory, Lund University, SE-221 00 Lund, Sweden
[3] Nano and Molecular Systems Research Unit, University of Oulu, FI-90014 Oulu, Finland
[4] Environmental and Chemical Engineering Research Unit, University of Oulu, FI-90014 Oulu, Finland
[5] Department of Physics, Lund University, SE-221 00 Lund, Sweden
[6] Department of Chemistry, University of Helsinki, FI-00014 Helsinki, Finland

[a)] **Author to whom correspondence should be addressed:** evgeniyr@smn.uio.no
[b)] **Current address:** Department of Chemistry and Materials Science, Aalto University, FI-00076 Aalto, Finland.

## ABSTRACT

An experimental approach is described in which well-defined perturbations of the gas feed into an Ambient Pressure X-ray Photoelectron Spectroscopy (APXPS) cell are fully synchronized with the time-resolved x-ray photoelectron spectroscopy data acquisition. These experiments unlock new possibilities for investigating the properties of materials and chemical reactions mediated by their surfaces, such as those in heterogeneous catalysis, surface science, and coating/deposition applications. Implementation of this approach, which is termed perturbation-enhanced APXPS, at the SPECIES beamline of MAX IV Laboratory is discussed along with several experimental examples including individual pulses of $N_2$ gas over a Au foil, a multi-pulse titration of oxygen vacancies in a pre-reduced $TiO_2$ single crystal with $O_2$ gas, and a sequence of alternating precursor pulses for atomic layer deposition of $TiO_2$ on a silicon wafer substrate.

*Published under license by AIP Publishing.* https://doi.org/10.1063/5.0039957

## I. INTRODUCTION

Exposure of solid surfaces to gaseous environments is an essential part of experimental studies in many disciplines including surface science, heterogeneous catalysis, materials science, or heterogeneous chemistry of aerosols. Gas treatments are used, for example, to remove surface contaminants, to alter the chemical composition of surfaces and/or adsorbed layers, to grow thin films, and, importantly, to perform surface-mediated (catalytic) chemical reactions. Exposure to gaseous stimuli can also be used to elicit various responses in the bulk of certain materials through electronic (current), mass (diffusion), or other forms of transport processes, which is relevant in sensing and energy conversion applications. Therefore, it is highly desirable to be able to exert precise control over the amount and temporal modality of gas exposure in combination with spectroscopic and structural characterization tools employed in fundamental studies of various materials. Experiments with well-defined transient perturbations (pulse, step, and periodic wave) are especially valuable, as they deliver more quantifiable real-time data about the investigated physico-chemical processes.

In chemical kinetics, transient gas perturbations are routinely employed to investigate the reaction mechanisms and derive the intrinsic reaction parameters of gas–surface interactions.[1–3] For example, step perturbations in the isotopic composition of the feed are used in Steady-State Isotopic Transient Kinetic Analysis (SSITKA) to evaluate the mean surface residence times and abundances of reaction intermediates.[4–6] Concentration step-transients

under flow conditions are widely used for kinetic investigations.[7] Periodic (pressure) waves are used in frequency methods to scrutinize the reaction kinetics under such operating conditions that may not be accessible to other transient methods.[8,9] Transient perturbations of the gas composition are also utilized in many spectroscopic and structural methods, e.g., Refs. 10–12, especially to enhance the sensitivity to such reaction intermediates that have their signals obscured by spectator species.[13–15]

This work derives motivation from Temporal Analysis of Products (TAP)—a powerful transient technique for the precise kinetic characterization of complex catalytic materials and reactions.[16,17] TAP employs nanomolar pulses of reactants that are injected over an evacuated sample (packed bed configuration) to probe its kinetic properties. Time-resolved (in the range of 1 ms) Quadrupole Mass-Spectrometry (QMS) responses of gaseous species are quantitatively analyzed, primarily within the model of Knudsen diffusion,[18] to extract a rich variety of intrinsic kinetic characteristics. Well-defined gas perturbations (pulses) also allow for the superior control over the chemical status of the catalyst surface.[16,17,19,20] When complemented by surface spectroscopy measurements on a comparable timescale, such pulse-response experiments can have profound implications for mechanistic studies in catalysis and materials science. For example, complementary spectro-kinetic data can be assimilated in a unified modeling framework, such as mean-field microkinetics or the Rate-Reactivity Model (RRM),[21] which improves our fundamental understanding of complex surfaces. Implementation of such perturbation-enhanced experiments in conjunction with surface-sensitive electron spectroscopies is particularly desirable for investigating correlations between the electronic structure and kinetic properties of materials.[22] However, this pursuit faces a number of technical and methodological challenges.

X-ray Photoelectron Spectroscopy (XPS) and Ultraviolet Photoelectron Spectroscopy (UPS) are essential surface-sensitive techniques that are widely applied for characterization of materials. Historically, Molecular Beam Scattering (MBS) methodology was utilized in conjunction with XPS and Infrared (IR) and Electron Energy Loss Spectroscopy (EELS) measurements in surface science as a mean to impose a well-defined gas perturbation, whereby the probe molecules are delivered onto a sample surface by using a focused molecular beam source in a continuous or periodic manner.[23,24] From the kinetics point of view, MBS experiments derive their strength from the well-defined, single-collision mode of gas transport in the free molecular flow regime, which facilitates quantitatively accurate estimations of intrinsic kinetic parameters from the time-resolved mass-spectrometric and spectroscopic signals.[25–27] When molecular beams are employed, gaseous species can be quantitatively monitored by using a mass-spectrometer in addition to monitoring surface species with spectroscopy. These combined spectro-kinetic data can be very informative for elucidating the reaction mechanisms on well-defined model surfaces, such as single crystals or thin films. However, MBS-enhanced spectroscopic experiments on model surfaces are limited in scope when it comes to investigating more structurally complex materials under technologically relevant operating conditions (e.g., higher pressure). Moreover, molecular beam sources and mass-spectrometers are rarely installed in the vicinity of the sample in conventional (commercial) XPS systems due to additional technical complexities. As a result, most surface spectroscopies are performed in high vacuum or in a static gas environment inside "back-filled" vacuum chambers. One notable example to the contrary is the Dynamic High Pressure (DHP) approach developed at the Elettra synchrotron,[28] in which gaseous pulse transients are employed to augment conventional XPS measurements. DHP utilizes short, intense pulses of gas to briefly expose the sample surface to elevated pressures of gaseous reactants. Although it may not be possible to acquire XPS spectra while such a pulse is in progress, they can readily be acquired in between the pulses to monitor the evolution of the surface within a series of pulses or to monitor the reactions of relatively long-lived adsorbents that remain on the surface immediately after a pulse.

Over the course of recent decades, a number of methodological and instrumentation advancements have opened new possibilities for *in situ* XPS investigations of chemically reactive surfaces, as recently reviewed by Schnadt *et al.*[29] Ambient Pressure XPS (APXPS) instruments (e.g., see Refs. 30–32 and references therein) have become commonplace at large synchrotron radiation facilities and, increasingly, in many home laboratories.[33] These instruments allow for the gas pressure in the vicinity of the sample surface to be increased up to 50–100 mbar, while still providing XPS spectra of high quality. This is achieved by placing a very narrow (100–1000 $\mu$m diameter) aperture of a differentially pumped electron analyzer only one or two aperture diameters away from the sample surface in order to minimize the escape path of the photoelectrons through the gas layer, while maintaining the elevated pressure of reactants at the sample surface. Subsequently developed small dead volume cells[34,35] feature a more rapid gas exchange within the cell volume—an essential pre-requisite for kinetically well-defined *in situ* APXPS experiments. The cutting edge APXPS cells with unique geometries[36] or capped with graphene membranes[37,38] achieve unprecedented high pressures up to several bars. Furthermore, highly sensitive detectors such as Delay Line Detectors (DLDs)[39,40] provide a sufficient signal-to-noise ratio for acquiring XPS spectra on the sub-second time scale. Other factors contributing to the improved data quality and temporal resolution include the high brilliance of synchrotron radiation and the high transmission of electron analyzers. Valuable kinetic insights about surface reactions have been gained by temperature-programmed APXPS measurements.[41] The aforementioned technological developments in photoelectron spectroscopies can potentially offer unprecedented experimental capabilities, whereby well-defined perturbations of the surrounding gas composition can be delivered to the model and complex materials, while their surfaces are simultaneously monitored by real-time XPS. We refer to this mode of experimentation as *perturbation-enhanced APXPS*, and the first examples of such experiments have already appeared for powdered catalysts in the recent literature.[42]

One of the practical challenges in conducting perturbation-enhanced XPS measurements is the synchronization of electronic components for precise gas control and data acquisition, which is crucial for achieving accurate temporal alignment of the resulting datasets and implementing advanced automation. We foresee that such a precise synchronization will become increasingly important for kinetically well-defined, TAP-like APXPS measurements. Here, we report the development of a hardware/software interface for performing well-defined, fully automated gas perturbations that are synchronized with the time-resolved XPS data acquisition.


Published under license by AIP Publishing

Selected experimental case studies are described to illustrate the potential application scope of these novel capabilities in the research of materials, evaluate their limits in the context of the state-of-the-art APXPS instruments, and discern the directions in which further developments could be fruitful.

## II. IMPLEMENTATION

Experiments were developed at the APXPS end station of the SPECIES beamline[43,44] at MAX IV Laboratory. The end station[35] is equipped with an ambient pressure XPS cell, a differentially pumped electron analyzer (SPECS Phoibos 150 NAP), and a DLD from Surface Concept. An Al/$Si_3N_4$ window mounted on the cell allows the x rays (either from an anode source or the synchrotron) to enter the cell without compromising the high vacuum conditions of the beamline and the rest of the vacuum system. The main aim of this work is to extend the capabilities of the instrument to enable simultaneous triggering (i.e., in the same time frame) of the gas perturbation by using an arbitrary injection device placed upstream of the AP cell and the XPS data acquisition by using the spectrometer.

### A. Hardware

Different components of the system are schematically depicted in Fig. 1 and include (1) a synchronizing controller interfaced with (2) an injection device and (3) DLD. The Raspberry Pi 3 unit (RPi)[45] that runs the Raspbian operating system was selected as the core of the system. RPi has many advantages in the context of this application, such as low price and compact dimensions, but the most important feature is its fully integrated general-purpose input/output (GPIO) circuit, which allows the RPi to easily interface with external equipment (see the circuit in Note 1 of the supplementary material).

Gases are supplied into the AP cell (inner volume ~200 ml) via two ~2 m long inlet lines (4 mm ID), both of which open into the conically shaped annulus surrounding the nozzle of the electron analyzer in order to deliver gas in close proximity of the sample surface. Pneumatically actuated diaphragm-sealed valves from Swagelok (model 6LVV-DPS4-C) were used as gas injectors upstream of the inlet lines, and their actuation was synchronized with the DLD data acquisition. Gases were evacuated from the back of the AP cell volume through an ~2 m long outlet line (4 mm ID) by using a turbo-molecular pump (pumping speed 67 l $s^{-1}$). The composition of the outlet gas stream was measured at the end of the outlet line by using a Quadrupole Mass-Spectrometer (QMS) via a variable leak valve. In order to control pressure inside the AP cell (measured by using a CERAVAC CTR 100 N capacitance pressure gauge at the outlet line, ~2 m from the cell and before the QMS entrance), a variable leak valve was placed upstream of the pneumatic valves. The leak rate was adjusted in advance to achieve the desired pressure in the cell and later kept at this constant opening during the experiment. The two pneumatic valves were operated in a dual mode with two configurations (see Fig. 2): (a) the inlet valve open and the bypass valve closed, which allows for gas injection into the AP cell, and (b) the inlet valve closed and the bypass valve open, which creates a gas-flow to the outlet pump and ensures no pressure build-up in the line. The bypass line was connected to the gas evacuation line of the APXPS end station pumped by using a turbo-molecular pump. The trigger signal was level-shifted to

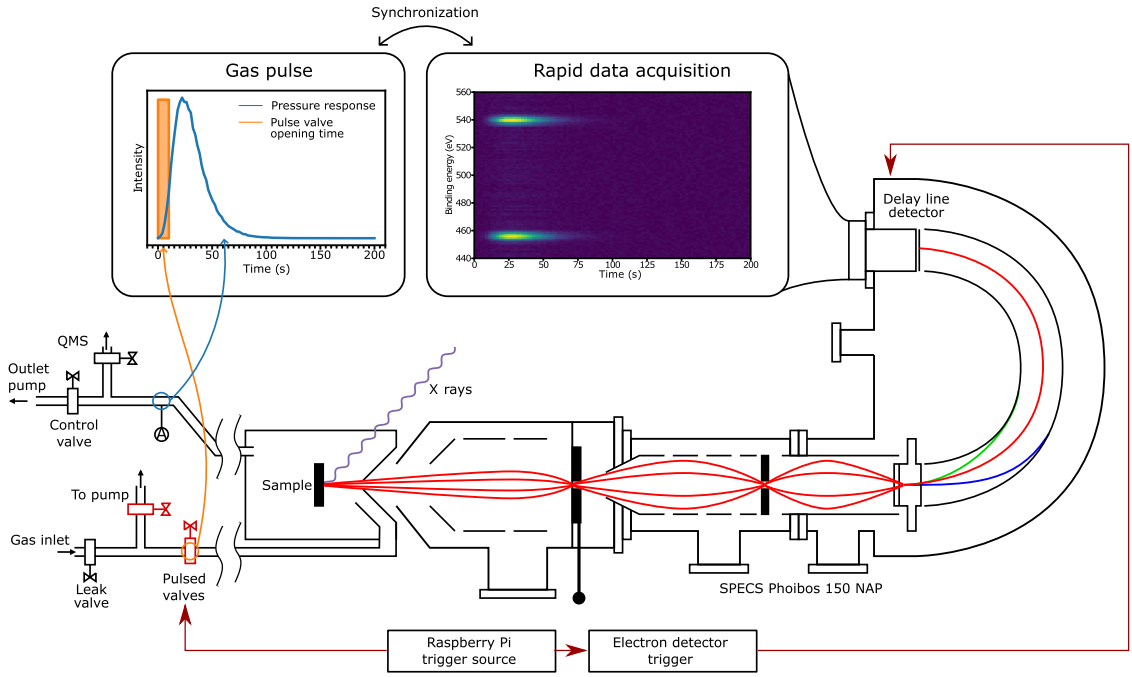


**FIG. 1.** A general scheme of the APXPS cell with a sample, the gas feeding section, and the electron analyzer. The insets show the imposed (square pulse) gas perturbation on the same time scale with the QMS signal at the cell outlet (left) and the synchronized DLD XPS signal recorded from the sample surface (right).


Published under license by AIP Publishing

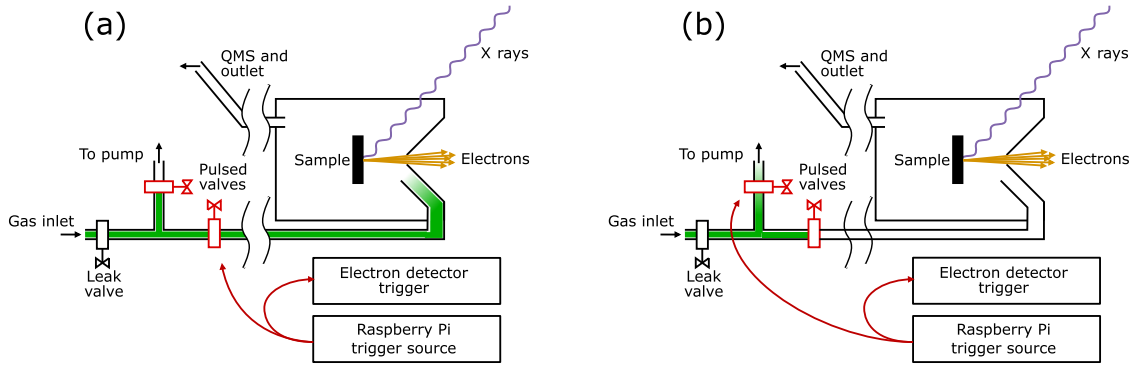


**FIG. 2.** The operating principles of pneumatic valves whose actuation was synchronized with the DLD via RPi: (a) gas injection mode and (b) gas bypass mode.

24 V with relays to operate the pneumatic valve actuators [shown in the upper right corner of Fig. S1(b) of the supplementary material], which were, in turn, controlled by using the RPi.

### B. Software

The control software was written in Python, which offers a wide variety of libraries for, among other things, the control of the RPi's GPIO circuit and user interfaces.[45,46] Python software was developed to (1) implement the gas injection sequences by triggering the pneumatic valves and (2) initiate the data acquisition by triggering the DLD. Some of the data acquisition parameters, such as the pass energy of the analyzer, are determined by the voltages applied to the spectrometer, which are set externally by the SpecsLab Prodigy software. The acquisition of the electron spectra by using the DLD, on the other hand, was controlled by a software provided by the Surface Concept GmbH. This data acquisition software records individual "snapshots" of the detector image when provided by an external trigger signal, which here was generated by using the RPi. The acquired images are converted into spectra by integrating over the non-dispersive (non-energy) axis. The energy scale is calibrated in a separate experiment with synchrotron light by measuring a known photoelectron line at different positions on the detector by changing the incident photon energy. This enables the calibration of the detector energy scale. Finally, the acquired APXPS spectra are aligned to the gas injection sequences in time by the time stamps in the data files.

## III. EXAMPLES OF APPLICATION IN APXPS EXPERIMENTS

The newly developed hardware/software interface was tested in three types of experiments, all of which have a potential to significantly enhance the studies of reactive materials at the SPECIES beamline: (1) pulse-response real-time analysis of gas and surface species, (2) pulsed titration of surface species for step-wise alteration of the surface composition, and (3) cycled exposure of surfaces to the Atomic Layer Deposition (ALD) precursors. Experiments were conducted in the "off-line" mode with a Mg K$\alpha$ x-ray source (SPECS XR50, 1253.6 eV, 250 W), which can be used in addition to synchrotron light at the APXPS end station.

### A. Time-resolved monitoring of gas and surface species

Monitoring the sample surface with XPS in real-time in response to a transient change in the gas composition is of great interest for applications in catalysis and surface chemistry. To demonstrate the perturbation-enhanced time-resolved data acquisition mode, nitrogen gas was injected over the gold foil, while XPS signals at N 1s and Au 4f binding energies were monitored as functions of time (see Fig. 3). Nitrogen gas does not react with gold under these conditions, making their combination a convenient model for elucidating the temporal characteristics of the signal in the absence of chemical reactions. The beginning of the injected square pulse [see Fig. 3(a)] defined the origin of the time axis (t = 0) for the DLD. The QMS located downstream (outlet line) from the AP cell was operated in a continuous data acquisition mode, and the QMS data were aligned with the DLD timeline postfactum based on the time stamps in the data files. The valve opening time (or pulse duration) $t_v$ served as the control parameter regulating pulse intensity. The pressure in the AP cell was adjusted using the variable leak valve to 1 mbar with the pulse valve fully open.

XPS responses of nitrogen gas (N 1s) above the sample surface and of the gold foil (Au 4f) are shown in Figs. 3(b) and 3(c), respectively. These data were recorded at 100 eV analyzer pass energy, 3 mm slit width, and 100 ms dwell time for each DLD image. Raw images (see, example, Note 2 of the supplementary material) were summed over all channels to produce time-resolved signals. Transient changes in both N 1s and Au 4f signals are distinguishable from the background already for the 1 s valve opening time, albeit with a low signal-to-noise ratio, and they become significantly more prominent for a longer valve opening. The inverted shape of the pulse in the Au 4f signal is due to the increased attenuation of photoelectrons from the surface by the injected $N_2$ gas molecules. Both N 1s and Au 4f signals in Figs. 3(b) and 3(c) were binned to the time resolution of 300 ms in order to improve the signal-to-noise ratio, which provided significant signal quality even though a Mg K$\alpha$ anode was used as the x-ray source. Synchrotron light is expected to afford even higher quality and time resolution of XPS spectra.

The N1s XPS signal for nitrogen gas can be directly compared to its QMS signal (amu 28) simultaneously recorded at the cell


Published under license by AIP Publishing

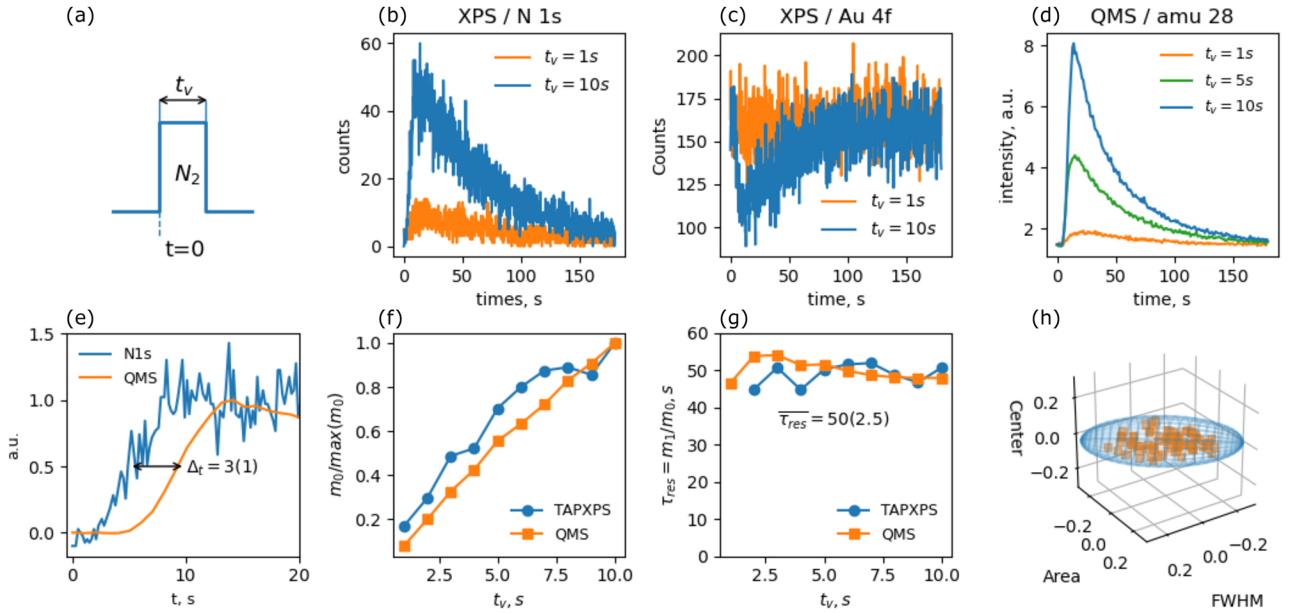


**FIG. 3.** A transient (pulse-response) APXPS experiment (Mg K$\alpha$ x-ray source) enabled by the synchronization interface: (a) temporal profile of the gas perturbation (pulse); (b) N 1s and (c) Au 4f transients recorded by using the DLD after single $N_2$ pulses over the gold foil, comparing responses for different valve opening times ($t_v$); (d) QMS signal at amu 28 recorded at the cell outlet for different $t_v$; (e) the time difference between the raising N 1s XPS vs QMS signals; (f) normalized zeroth moments and (g) mean residence times of N 1s XPS (DLD) and QMS signals as functions of valve opening times $t_v$; and (h) reproducibility of pulse characteristics (relative deviations from the sample-mean values of the center, size, and width). The ovoid depicts the maximal encompassing volume for the entire dataset.

outlet. As shown in Fig. 3(d), QMS signals generally reproduce the same pulse shape as N 1s signals, but with a much higher signal-to-noise ratio. Closer inspection [see Fig. 3(e)] of the rising pulse edge for height-normalized signals reveals that the QMS response is consistently delayed with respect to the XPS response by 3(±1) s. This delay can be attributed to the increased (doubled) distance in the gas lines between the injection point and the QMS as compared to the injection point and the sample, which is in good agreement with the delay expected based on the vacuum conductance of the outlet line under these conditions (see Note 3 of the supplementary material).

To further characterize the XPS and QMS signals, zeroth ($m_0$) and first ($m_1$) statistical moments were calculated for all transients after baseline correction (see Note 2 of the supplementary material). Zeroth moments (i.e., area under the curve) are proportional to the amount of injected gas molecules (pulse size). Figure 3(f) demonstrates that the pulse size (normalized $m_0$) increases linearly with the increasing valve opening time ($t_v$) and that both QMS and XPS signals respond to this increase with comparable sensitivity. However, we note that the XPS-derived zeroth moment exhibits higher uncertainty due to its lower signal-to-noise ratio.

Both signals yield approximately the same mean residence time of gas molecules in the AP cell ($\tau_{res}$) of 50(±2.5) s, which is independent of the valve opening time [Fig. 3(g)]. A comparison of the mean residence time and the average rising pulse edge delay of the QMS (50 s ≫ 3 s) suggests that the majority of molecules primarily reside within the AP cell, where they collide extensively with each other and with the cell walls before being evacuated either through the outlet or the nozzle of the electron analyzer. This is the characteristic of a device with considerable degree of mixedness, despite the presence of relatively long inlet and outlet pipes.

Reproducibility of perturbations is another highly desirable per-requisite for systematic transient kinetic experiments. In order to assess pulse reproducibility, a series of 80 pulses ($t_v$ = 4.5 s) were supplied into the cell under otherwise constant conditions, and the variances of the corresponding responses were analyzed within the sequence. The response shapes were regressed (Levenberg–Marquardt algorithm) using a combination of a linear background and an exponential Gaussian pulse as a model (see Note 2 of the supplementary material). The three independent parameters in this simple model (i.e., the pulse size, the mean delay, and the variance) were not strongly correlated with either each other or the pulse order within the sequence and were normally distributed around their mean values. Figure 3(h) illustrates a scatter plot of all 80 pulses, as relative deviations from the sample-mean, in three principal parametric dimensions: area, FWHM, and mean delay. The dataset is scattered along the area and mean delay axes only within the 10% radius, although it is more broadly scattered along the FWHM axis (within 20%).

The amount of gas molecules injected per pulse can be estimated from the known flow rate of 1 SCCM ($10^{-6}$/60 $m^3$/s) and pressure of 1 mbar (100 Pa) that were observed at steady-state feed conditions prior to the pulsing experiment, i.e., with the pulsing valve fully open. Assuming the ideal gas law, the amount of molecules injected at the valve opening time of 1 s ($t_v$ = 1 s) can be estimated as


Published under license by AIP Publishing

$$N_p = t_v \cdot \frac{Pv}{RT} = 1\ \mathrm{s} \cdot \frac{100\ \mathrm{Pa} \cdot (1.0/60) \cdot 10^{-6}}{300\ \mathrm{K} \cdot 8.314} \approx 1 \cdot 10^{-9} \mathrm{mol}. \quad (1)$$

We note that this estimate provides an upper bound of the pulse size since in reality, the pressure may not reach 1 mbar during the entire valve opening period due to a finite transient time. This "order-of-magnitude" estimate falls within the typical range of TAP experiments, which further illustrates that TAP and APXPS operate at similar pressure/temperature conditions and can potentially be combined in a fully reconciled transient spectro-kinetic experiment, albeit it is likely that despite considerable residence time in the cell, not all gas molecules collide with the sample surface.

The overall reproducibility of pulses and the robustness of simple phenomenological pulse descriptors (Fig. 3) achieved in this work constitute an important step toward the development of spectro-kinetic approaches involving APXPS. The inert gas-phase and surface tracer responses presented herein are already amenable to simple kinetic estimations within specified uncertainties. More systematic tracer studies would be necessary to fully understand the model of gas transport within the AP cell, highlighting the need for well-defined gas transport conditions that can be employed as standard processes for precise kinetic measurements, similarly to Knudsen diffusion in TAP. Nevertheless, the phenomenological values provided in this work for the mean (transport) residence time of gas inside the AP cell (including the gas lines) can readily be used to constrain the range of characteristic time scales for (chemical) kinetics that can be quantified under the used experimental conditions. Assuming an ideally mixed reaction volume, i.e., Continuous Stirred-Tank Reactor (CSTR) in the AP cell, for which conversion is given[3] by

$$X = \frac{k_{app}\tau}{1 + k_{app}\tau}, \quad (2)$$

a device with the mean residence time $\tau$ of 50 s can potentially provide kinetically meaningful data (still subject to other, more stringent, criteria) with conversions between 0.05 and 0.95 for chemical processes with characteristic apparent rate constants $k_{app}$ of $10^{-3}$–10 $s^{-1}$. The corresponding range of intrinsic rate constants $k$, $m^3\ mol^{-1}\ s^{-1}$ can be estimated by taking into account a typical surface-to-volume ratio $S_V$ in the AP cell (for a $5 \cdot 10^{-5}$ $m^2$ sample inside the $0.2 \cdot 10^{-3}$ $m^3$ AP cell) and a typical site-density $a_S$ on a metal surface of $1 \cdot 10^{-6}$ mol $m^{-2}$,

$$k = \frac{k_{app}}{a_S S_V}, \quad (3)$$

resulting in the $k$ range of ~$10^3$ to $10^6$ $m^3\ mol^{-1}\ s^{-1}$. In the context of heterogeneous catalysis, this range of values would correspond to extremely fast processes, comparable to the rates of oxygen dissociation on Pt at similar conditions.[47] These order-of-magnitude estimates indicate that kinetically relevant transient APXPS experiments for a wide range of catalytic reactions with lower intrinsic rate constants can be implemented if the surface-to-volume ratio in the AP cell is considerably increased, for example, by employing samples comprised of porous films. For significantly slower reactions, the cell volume must also be reduced. For example, at 423 K, methanol reacts with oxygen atoms adsorbed on a surface of nanoporous gold with an intrinsic rate constant[48,49] of $k \sim 10^2$ $m^3\ mol^{-1}\ s^{-1}$. Considering that the realistic oxygen coverage on this material is limited to fractions of a monolayer (0.01ML) due to the low oxygen dissociation probability, the apparent rate constant of this reaction would reach the lower bound of the sensitivity window if the volume of the cell is reduced to $2 \cdot 10^{-6}$ $m^3$, while the surface area is increased to $1 \cdot 10^{-4}$ $m^2$,

$$k_{app} = k a_S S_V = \frac{10^2 \cdot 0.01 \cdot 2.3 \cdot 10^{-5} \cdot 10^{-4}}{2 \cdot 10^{-6}} = 1 \cdot 10^{-3} s^{-1}, \quad (4)$$

where $2.3 \cdot 10^{-5}$ mol $m^{-2}$ is the atomic monolayer of a model Au(111) surface.

Aside from increasing the surface-to-volume ratio in the AP cell, experiments reported herein suggest potential avenues for further methodological improvements. Perturbations with even better control over the injected amounts, reproducibility, and gas transport times, comparable to those of TAP and modulation excitation techniques, could be achieved with deeper integration of hardware components in future instruments, e.g., installing the gas injection valves in the immediate vicinity of the sample.

### B. Pulse-wise titration of surface species

Monitoring the evolution of the sample surface within a series of many successive pulses is another useful mode of operation for the developed pulsing capabilities. This allows for the controlled preparation of specific surface states and systematic studies of surface changes (i.e., titration or well-defined state-altering TAP-like experiments[50]). To illustrate this operation mode, re-oxidation of a partially reduced titanium oxide surface was used as an example (Fig. 4). $TiO_2$ is a highly relevant material in (photo)catalysis[51] and aerosol science,[52,53] where its chemical properties are greatly affected by the surface oxidation state.

In this work, a single crystal of the rutile $TiO_2$ exposing (110) surface (supplier: PI-KEM) was first reduced by $Ar^+$ ion sputtering (1.5 kV, 10 mA, $2 \cdot 10^{-5}$ mbar Ar, 20 min), which created oxygen vacancies. Then, the surface was gradually re-oxidized by injecting a train of $O_2$ pulses (1 s valve opening time, 60 s between pulses), while monitoring Ti 2p XPS spectra with the DLD at an analyzer pass energy of 50 eV, 3 mm slit width, and 100 ms dwell time for the image acquisition. The initial reduction and subsequent pulse-wise re-oxidation of the titania (110) surface are reflected prominently in its Ti 2p spectra, as shown in Fig. 4(a). Here, non-transient high-resolution Ti 2p XPS spectra are plotted for the initial (fully oxidized, UHV reference), sputtered (deeply reduced), and partially re-oxidized (after 20 room temperature $O_2$ pulses) states of titania. Different oxidation states of Ti can clearly be distinguished in these spectra, in agreement with reference data on bulk materials[54] and recent APXPS measurements on Ti(110).[55] The spectrum of fully oxidized $TiO_2$ (UHV reference) is composed of a characteristic $Ti^{4+}$ doublet (due to spin–orbit coupling) with the more intense $Ti^{4+}$ $2p^{3/4}$ component centered at 459.7 eV and a less intense $Ti^{4+}$ $2p^{1/2}$ component centered at 465.5 eV, without any signs of $Ti^{3+}$. The spectrum of sputtered titania features an additional spin–orbit pair of $Ti^{3+}$ 2p components, which are shifted with respect to $Ti^{4+}$ to lower binding energies. In the partially re-oxidized spectrum, the intensity ratio between the two predominant oxidation states $Ti^{4+}/Ti^{3+}$ is shifted back toward the fully oxidized UHV reference. Even without rigorous deconvolution of these complex spectra, which was not pursued in these proof of principle studies, it can be


Published under license by AIP Publishing

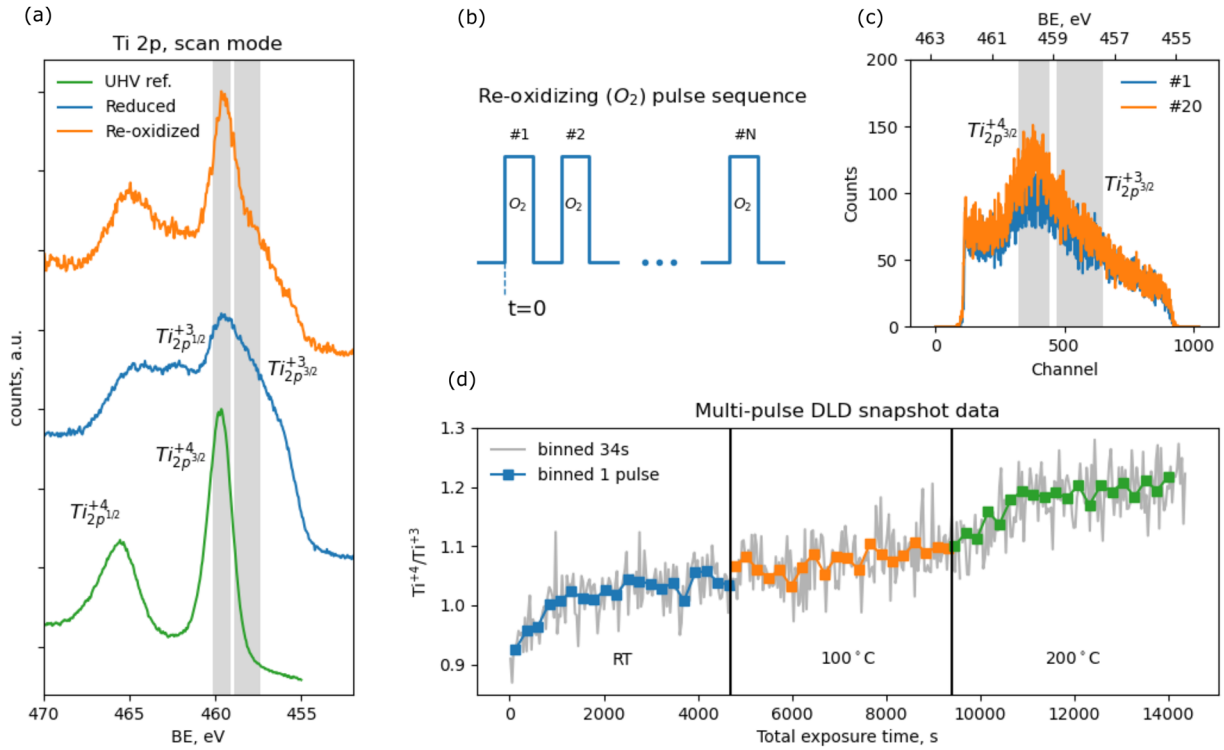


**FIG. 4.** A multi-pulse APXPS experiment (Mg K$\alpha$ x-ray source) with re-oxidation of pre-reduced $TiO_2$ (110) single crystal. (a) High-resolution scans of the initial fully oxidized surface in UHV (bottom), partially reduced, sputtered surface (middle), and partially re-oxidized surface after $O_2$ pulses. (b) A schematic representation of the pulsing sequence used for the crystal re-oxidation. (c) Examples of raw DLD spectra after the first and 20th pulses. (d) The nominal $Ti^{4+}/Ti^{3+}$ ratio as a function of $O_2$ exposure at various temperatures. Data binned to 34 s (gray line) and 1 individual pulse (blue squares) to illustrate the trade-off between the temporal resolution and signal-to-noise ratio. The $Ti^{4+}/Ti^{3+}$ ratio was obtained by integrating the corresponding spectral regions that are highlighted in gray in (a) and (c).

seen that the ratio between the integrated intensities within the $Ti^{4+}$ and $Ti^{3+}$ bands ($Ti^{4+}/Ti^{3+}$) can be used as a descriptor of the average surface oxidation state.

To quantify the average surface oxidation state during the re-oxidation pulse sequence, the acquired raw DLD spectra were binned in time and integrated in two spectral regions representative of the $Ti^{4+}$ species (channels 320–440 or 460.14–459.13 eV) and $Ti^{3+}$ species (channels 470–650 or 458.88–457.38 eV). These spectral ranges are highlighted in Fig. 4(c) for DLD snapshots and in Fig. 4(a) for reference spectra. The initial state of sputtered, partially reduced $TiO_2$ was characterized by the ratio of $Ti^{4+}/Ti^{3+}$ spectral regions of 0.9 in the raw DLD data, which agreed well with the corresponding ratio of 0.86 in the full scan [Fig. 4(a)]. The evolution of the $Ti^{4+}/Ti^{3+}$ ratio during an ensuing series of oxygen pulses demonstrated the ability to precisely control the oxidation state of the titania surface within the 0.9–1.2 range of the $Ti^{4+}/Ti^{3+}$ ratio. The resulting nominal $Ti^{4+}/Ti^{3+}$ ratio increased with the number of injected oxygen pulses, as expected from the re-oxidation process [see Fig. 4(d)]. Furthermore, several regimes in the re-oxidation kinetics could be clearly distinguished: the initial rapid increase in the $Ti^{4+}/Ti^{3+}$ ratio during the first five pulses at room temperature, followed by a slower (linear) increase with the slope largely unaffected by the temperature change from room temperature to 100 °C. A similar pattern was observed again, while the material was further re-oxidized at a higher temperature of 200 °C. A comparison with the fully oxidized UHV reference in Fig. 4(a), which exhibited a nominal $Ti^{4+}/Ti^{3+}$ descriptor ratio of 2 despite not containing $Ti^{+3}$ (integration artifact), reveals that the surface was not completely oxidized into original stoichiometric $TiO_2$ by the end of the pulse sequence at 200 °C. It should be noted, however, that this comparison is also affected by the difference in backgrounds in the two data acquisition modes.

Drawing parallels with multi-pulse TAP experiments, the sequence-based experimental approach in APXPS presents novel opportunities for the systematic characterization of chemically reactive and dynamically evolving surfaces. For example, the rate of O-vacancy diffusion from the bulk of the material can be evaluated by monitoring the chemical state of the surface with XPS after a pre-defined number of pulses have been delivered. Likewise, pulse sequences of reagent molecules can be used to prepare and probe chemical properties of well-defined surface states in catalysis, e.g., see the work of Shekhtman *et al.*[50] or Wang and Makkee.[56] We note that in the specific example of multi-pulse data presented in Fig. 4, the evolution of the titania surface occurred on relatively slow time scale, which could have been captured by the less time-resolved data acquisition mode. However, in the future, the newly developed


Published under license by AIP Publishing

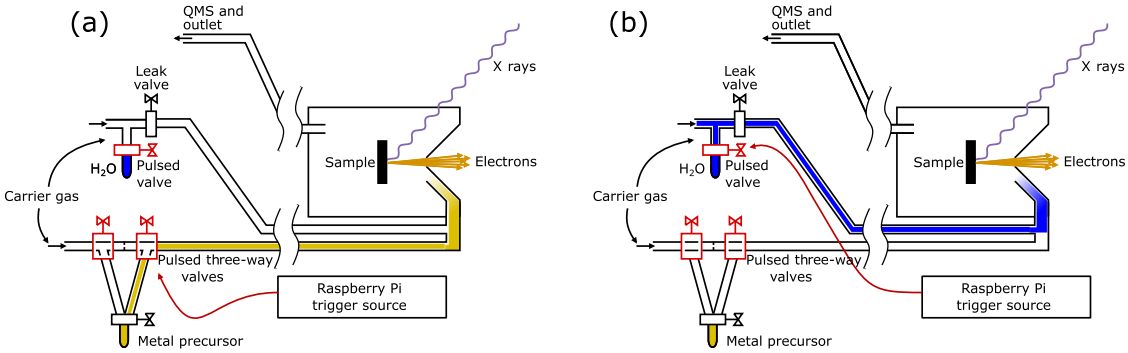


**FIG. 5.** The operation of pneumatic valves during ALD half-cycles: (a) metal precursor injection and (b) water injection.

synchronization capabilities will facilitate quantitative reconciliation of the kinetic and spectroscopic data related to a broader range of reaction kinetics.

### C. Precursor delivery for atomic layer deposition (ALD)

A pulsed valve system similar to the one described in this paper is commonly employed in Atomic Layer Deposition (ALD) processes.[57] In ALD, a substrate is exposed periodically and alternatingly to different precursor gases, which create—under ideal conditions—atomically thin, conformal layers of materials, depending on the precursors used. Thicknesses of these films can be controlled accurately and simply by the number of deposition cycles repeated. APXPS measurements have emerged as a valuable source of fundamental information about the surface reactions involved in ALD.[58–61] We have used the pulsed valve system together with the RPi electronics to automate the pulsing of the precursor gases in order to study ALD processes *in situ* using APXPS.

For the ALD experiments, the gas lines and the pulsed valves were slightly re-configured from the experiments described above, as shown in Fig. 5. In this case, there had to be two inlet tubes to the AP cell, one for each precursor and at least one pulsed valve in each inlet tube in order to supply reagents for the both ALD half-cycles. Likewise, the Python script controlling the valves was adjusted to implement the sequential injection of ALD precursors. As the programming is done fully in the Python environment, it is easily adaptable to different applications and relatively quick to reprogram in order to meet different experimental needs and more complicated pulsing sequences. In this case, the program emulated pulse-purge-pulse-purge cycles of an ALD process, in which titania ($TiO_2$) layers were grown on a silicon substrate at 200 °C.

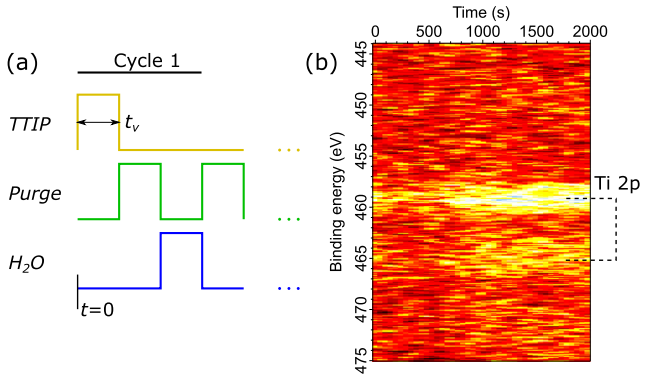


**FIG. 6.** Use of synchronized valves for ALD: (a) the pulsing sequence used for $TiO_2$ deposition and (b) time-resolved APXPS data during the TTIP precursor pulse recorded using the Mg Kα x-ray source.

The pulsing sequence [see Fig. 6(a)] consisted of an exposure to titanium (IV) tetraisopropoxide (TTIP)—the source of titanium—followed by a period of purging with inert gas of the cell, and then followed by an exposure to water—the source of oxygen. A final purge period completed the cycle, after which another ALD cycle could begin. Figure 6(b) demonstrates an example of APXPS data recorded during the first (TTIP) half-cycle ($t_v$ = 2000 s). XPS was measured in a snapshot mode, with a fixed kinetic energy window focusing on the Ti 2p region at a binding energy of ~460 eV. A considerable delay between the pulse injection and the appearance of the surface Ti signal in XPS is caused by the reaction of the TTIP precursor with surfaces of the feed lines and the APXPS cell that have either never been exposed to the precursor before or have been exposed to water prior to the TTIP injection. The $TiO_2$ growth on the sample surface is observed only after all preceding surfaces are saturated with the precursor.

Overall, this example clearly demonstrates the utility of programmable perturbations of gas composition fully synchronized with the APXPS data acquisition for reproducibility of ALD cycles in the APXPS spectroscopic cell and, potentially, for acquiring time-resolved APXPS data on the kinetics of ALD growth reactions. One must note, though, that the time constants of the cell are still too large to capture kinetics of the most relevant ALD processes that are completed in fractions of seconds in actual ALD reactors. In other words, the current setup appears to operate in a transport-limited rather than reaction-limited mode. Therefore, the main value of these experiments is expected to lie in the chemical identification of the surface intermediates formed in each ALD reaction step.

## IV. CONCLUSION AND PERSPECTIVES

A hardware/software interface is described that allows for the injection of well-defined gas pulses into an APXPS cell on the


Published under license by AIP Publishing

same time frame, i.e., fully synchronized, with the triggering of a DLD XPS system. This interface enables a number of fast, time-resolved, perturbation-enhanced APXPS experiments to be systematically performed with a wide variety of materials and reactions. The synchronizing interface was implemented at the APXPS branch of the SPECIES beamline at MAX IV Laboratory based on a Raspberry Pi controller with a Python API and a number of other easily accessible components. The capabilities of this approach were illustrated by three experimental examples. First, $N_2$ pulsing over the Au foil demonstrated that XPS signals, in this case N 1s and Au 4f, can be monitored with sub-second time resolution for a single gas pulse. In combination with downstream QMS data, these pulses demonstrated that the APXPS cell has a characteristic residence time of 50 s, which can tentatively be assigned to the inner well-mixed volume of the cell, rather than the upstream and downstream feed lines. Second, Ti 2p XPS spectra recorded during a multi-pulse sequence of $O_2$ injections over pre-reduced $TiO_2$ were used to quantitatively monitor the evolution of the Ti oxidation state, which revealed a non-trivial behavior of re-oxidation kinetics. Finally, time-resolved XPS data were presented for the precursor-loading half-cycle of an ALD process for $TiO_2$ deposition.

Although developed for model systems already in the early days of surface science, such experiments with synchronous gas perturbations and surface characterization have not found their way into the standard repertoire of modern APXPS measurements, partially because the methodology development efforts were primarily focused on maximizing the pressure of reactants in the vicinity of the sample. Perturbation-enhanced APXPS experiments developed herein were inspired by the success of pulse-response TAP experiments in elucidating the intrinsic kinetics of gas–solid reactions on complex materials from a gaseous perspective. We foresee that the perturbation-enhanced APXPS approach will provide complementary time-resolved data from a surface perspective, which eventually can be reconciled with gaseous reaction kinetics for a more in depth understanding of underlying structure–activity relationships in catalysis and beyond.

## SUPPLEMENTARY MATERIAL

See the supplementary material for the detailed descriptions of (1) the synchronization circuitry, (2) data treatment that was employed in the analysis of gas pulses and (3) estimates of the vacuum pipe conductance.

## AUTHORS' CONTRIBUTIONS

E.A.R. and N.J. contributed equally to this work.

## ACKNOWLEDGMENTS

This work was funded by the Research Council of Norway (RCN) under Contract No. 272266 (TAPXPS project) and the European Regional Development Fund (Interreg Öresun-Kattegat-Skagerrak ESS & MAX IV: Cross Border Science and Society, MAX4ESSFUN, Ref. No. MAX-004). S.U. acknowledges funding from the European Research Council under the European Union's Horizon 2020 research and innovation program, Project SURFACE (Grant Agreement No. 717022), and the Academy of Finland (Grant No. 326291). The ALD-related research was financed by the Faculty of Science, University of Helsinki, and the Academy of Finland (Grant Nos. 295696 and 309552). We acknowledge MAX IV Laboratory for time on the SPECIES beamline. Research conducted at MAX IV, a Swedish national user facility, was supported by the Swedish Research council under Contract No. 2018-07152, the Swedish Governmental Agency for Innovation Systems under Contract No. 2018-04969, and Formas under Contract No. 2019-02496. The authors acknowledge technical support from many colleagues at MAX-IV and UiO. Last, but not least, the authors would like to express their gratitude for many inspiring discussions with Professor John Gleaves and Mr. John Gleaves, Jr. of Mithra Technologies (USA), Dr. Rebecca Fushimi of Idaho National Laboratory (USA), Professor Joachim Schnadt of Lund University (Sweden), and Dr. Spyros Diplas of SINTEF Industry (Norway), which contributed to finding many solutions, asking even more questions, and maintaining the spirit of adventure during this work.

## DATA AVAILABILITY

The data that support the findings of this study are available from the corresponding author upon reasonable request.

## REFERENCES

[1]C. O. Bennett, "Understanding heterogeneous catalysis through the transient method," in *Catalysis Under Transient Conditions*, edited by A. T. Bell and L. L. Hegedus (American Chemical Society, Washington, DC, 1982), Vol. 178, pp. 1–32.

[2]K. Tamaru, "Dynamic relaxation methods in heterogeneous catalysis," in *Catalysis: Science and Technology*, Catalysis, edited by J. R. Anderson and M. Boudart (Springer, Berlin, Heidelberg, 1991), pp. 87–129.

[3]G. B. Marin and G. S. Yablonsky, *Kinetics of Chemical Reactions: Decoding Complexity* (Wiley-VCH, 2011).

[4]J. Happel, "Transient tracing," Chem. Eng. Sci. **33**(11), 1567 (1978).

[5]S. L. Shannon and J. G. Goodwin, "Characterization of catalytic surfaces by isotopic-transient kinetics during steady-state reaction," Chem. Rev. **95**(3), 677–695 (1995).

[6]C. Ledesma, J. Yang, D. Chen, and A. Holmen, "Recent approaches in mechanistic and kinetic studies of catalytic reactions using SSITKA technique," ACS Catal. **4**(12), 4527–4547 (2014).

[7]A. Bundhoo, J. Schweicher, A. Frennet, and N. Kruse, "Chemical transient kinetics applied to CO hydrogenation over a pure nickel catalyst," J. Phys. Chem. C **113**(24), 10731–10739 (2009).

[8]Y. Yasuda, H. Mizusawa, and T. Kamimura, "Frequency response method for investigation of kinetic details of a heterogeneous catalyzed reaction of gases," J. Phys. Chem. B **106**(26), 6706–6712 (2002).

[9]V. P. Zhdanov, "Periodic perturbation of the kinetics of heterogeneous catalytic reactions," Surf. Sci. Rep. **55**(1), 1–48 (2004).

[10]J. Scalbert, F. C. Meunier, C. Daniel, and Y. Schuurman, "An operando DRIFTS investigation into the resistance against $CO_2$ poisoning of a Rh/alumina catalyst during toluenehydrogenation," Phys. Chem. Chem. Phys. **14**(7), 2159–2163 (2012).

[11]M. A. Newton, "Time resolved operando x-ray techniques in catalysis, a case study: CO oxidation by $O_2$ over Pt surfaces and alumina supported Pt catalysts," Catalysts **7**(2), 58 (2017).

[12]I. B. Minova, S. K. Matam, A. Greenaway, C. R. A. Catlow, M. D. Frogley, G. Cinque, P. A. Wright, and R. F. Howe, "Elementary steps in the formation of hydrocarbons from surface methoxy groups in HZSM-5 seen by synchrotron infrared microspectroscopy," ACS Catal. **9**(7), 6564–6570 (2019).

[13]A. Urakawa, T. Bürgi, and A. Baiker, "Sensitivity enhancement and dynamic behavior analysis by modulation excitation spectroscopy: Principle and application in heterogeneous catalysis," Chem. Eng. Sci. **63**(20), 4902–4909 (2008).


Published under license by AIP Publishing

[14]D. Ferri, M. A. Newton, and M. Nachtegaal, "Modulation excitation x-ray absorption spectroscopy to probe surface species on heterogeneous catalysts," Top. Catal. **54**(16-18), 1070–1078 (2011).
[15]D. Baurecht and U. P. Fringeli, "Quantitative modulated excitation Fourier transform infrared spectroscopy," Rev. Sci. Instrum. **72**(10), 3782–3792 (2001).
[16]J. T. Gleaves, J. R. Ebner, and T. C. Kuechler, "Temporal analysis of products (TAP)—A unique catalyst evaluation system with submillisecond time resolution," Catal. Rev. **30**(1), 49–116 (1988).
[17]J. T. Gleaves, G. Yablonsky, X. Zheng, R. Fushimi, and P. L. Mills, "Temporal analysis of products (TAP)—Recent advances in technology for kinetic analysis of multi-component catalysts," J. Mol. Catal. A: Chem. **315**(2), 108–134 (2010).
[18]G. S. Yablonsky, M. Olea, and G. B. Marin, "Temporal analysis of products: Basic principles, applications, and theory," J. Catal. **216**(1-2), 120–134 (2003).
[19]K. Morgan, N. Maguire, R. Fushimi, J. T. Gleaves, A. Goguet, M. P. Harold, E. V. Kondratenko, U. Menon, Y. Schuurman, and G. S. Yablonsky, "Forty years of temporal analysis of products," Catal. Sci. Technol. **7**(12), 2416–2439 (2017).
[20]D. Widmann and R. J. Behm, "Activation of molecular oxygen and the nature of the active oxygen species for CO oxidation on oxide supported Au catalysts," Acc. Chem. Res. **47**(3), 740–749 (2014).
[21]G. S. Yablonsky, E. A. Redekop, D. Constales, J. T. Gleaves, and G. B. Marin, "Rate-reactivity model: A new theoretical basis for systematic kinetic characterization of heterogeneous catalysts," Int. J. Chem. Kinet. **48**(6), 304–317 (2016).
[22]K. Roy, L. Artiglia, and J. A. van Bokhoven, "Ambient pressure photoelectron spectroscopy: Opportunities in catalysis from solids to liquids and introducing time resolution," ChemCatChem **10**(4), 666–682 (2018).
[23]G. W. Rubloff, "Photoemission studies of time-resolved surface reactions: Isothermal desorption of CO from Ni(111)," Surf. Sci. **89**(1), 566–574 (1979).
[24]F. Steinbach and J. Schütte, "Time-resolved photoelectron spectroscopy for the study of dynamic surface species," Rev. Sci. Instrum. **54**(9), 1169–1174 (1983).
[25]M. P. D'Evelyn and R. J. Madix, "Reactive scattering from solid surfaces," Surf. Sci. Rep. **3**(8), 413–495 (1983).
[26]J. Libuda, "Molecular beams and model catalysis: Activity and selectivity of specific reaction centers on supported nanoparticles," Chemphyschem **5**(5), 625–631 (2004).
[27]F. Zaera, "Use of molecular beams for kinetic measurements of chemical reactions on solid surfaces," Surf. Sci. Rep. **72**(2), 59–104 (2017).
[28]M. Amati, M. K. Abyaneh, and L. Gregoratti, "Dynamic high pressure: A novel approach toward near ambient pressure photoemission spectroscopy and spectromicroscopy," J. Instrum. **8**(05), T05001 (2013).
[29]J. Schnadt, J. Knudsen, and N. Johansson, "Present and new frontiers in materials research by ambient pressure x-ray photoelectron spectroscopy," J. Phys.: Condens. Matter **32**, 413003 (2020).
[30]M. Salmeron and R. Schlogl, "Ambient pressure photoelectron spectroscopy: A new tool for surface science and nanotechnology," Surf. Sci. Rep. **63**(4), 169–199 (2008).
[31]L. Trotochaud, A. R. Head, O. Karslıoğlu, L. Kyhl, and H. Bluhm, "Ambient pressure photoelectron spectroscopy: Practical considerations and experimental frontiers," J. Phys.: Condens. Matter **29**(5), 053002 (2016).
[32]L. Nguyen, F. F. Tao, Y. Tang, J. Dou, and X.-J. Bao, "Understanding catalyst surfaces during catalysis through near ambient pressure x-ray photoelectron spectroscopy," Chem. Rev. **119**(12), 6822–6905 (2019).
[33]C. Arble, M. Jia, and J. T. Newberg, "Lab-based ambient pressure x-ray photoelectron spectroscopy from past to present," Surf. Sci. Rep. **73**(2), 37–57 (2018).
[34]J. Knudsen, J. N. Andersen, and J. Schnadt, "A versatile instrument for ambient pressure x-ray photoelectron spectroscopy: The Lund cell approach," Surf. Sci. **646**, 160–169 (2016).
[35]J. Schnadt, J. Knudsen, J. N. Andersen, H. Siegbahn, A. Pietzsch, F. Hennies, N. Johansson, N. Mårtensson, G. Öhrwall, S. Bahr, S. Mähl, and O. Schaff, "The new ambient-pressure X-ray photoelectron spectroscopy instrument at MAX-Lab," J. Synchrotron Radiat. **19**(5), 701–704 (2012).
[36]P. Amann, D. Degerman, M.-T. Lee, J. D. Alexander, M. Shipilin, H.-Y. Wang, F. Cavalca, M. Weston, J. Gladh, M. Blom, M. Björkhage, P. Löfgren, C. Schlueter, P. Loemker, K. Ederer, W. Drube, H. Noei, J. Zehetner, H. Wentzel, J. Åhlund, and A. Nilsson, "A high-pressure x-ray photoelectron spectroscopy instrument for studies of industrially relevant catalytic reactions at pressures of several bars," Rev. Sci. Instrum. **90**(10), 103102 (2019).
[37]M. Salmeron, "From surfaces to interfaces: Ambient pressure XPS and beyond," Top. Catal. **61**(20), 2044–2051 (2018).
[38]J. J. Velasco-Vélez, V. Pfeifer, M. Hävecker, R. Wang, A. Centeno, A. Zurutuza, G. Algara-Siller, E. Stotz, K. Skorupska, D. Teschner, P. Kube, P. Braeuninger-Weimer, S. Hofmann, R. Schlögl, and A. Knop-Gericke, "Atmospheric pressure X-ray photoelectron spectroscopy apparatus: Bridging the pressure gap," Rev. Sci. Instrum. **87**(5), 053121 (2016).
[39]H. Keller, G. Klingelhöfer, and E. Kankeleit, "A position sensitive microchannelplate detector using a delay line readout anode," Nucl. Instrum. Methods Phys. Res., Sect. A **258**(2), 221–224 (1987).
[40]M. Lampton, O. Siegmund, and R. Raffanti, "Delay line anodes for microchannel-plate spectrometers," Rev. Sci. Instrum. **58**(12), 2298–2305 (1987).
[41]C. J. (Kees-Jan) Weststrate, D. Sharma, D. Garcia Rodriguez, M. A. Gleeson, H. O. A. Fredriksson, J. W. Niemantsverdriet, and J. W. (Hans) Niemantsverdriet, "Mechanistic insight into carbon-carbon bond formation on cobalt under simulated Fischer-Tropsch synthesis conditions," Nat. Commun. **11**(1), 750 (2020).
[42]L. Artiglia, F. Orlando, K. Roy, R. Kopelent, O. Safonova, M. Nachtegaal, T. Huthwelker, and J. A. van Bokhoven, "Introducing time resolution to detect $Ce^{3+}$ catalytically active sites at the $Pt/CeO_2$ interface through ambient pressure x-ray photoelectron spectroscopy," J. Phys. Chem. Lett. **8**(1), 102–108 (2017).
[43]S. Urpelainen, C. Såthe, W. Grizolli, M. Agåker, A. R. Head, M. Andersson, S.-W. Huang, B. N. Jensen, E. Wallén, H. Tarawneh, R. Sankari, R. Nyholm, M. Lindberg, P. Sjöblom, N. Johansson, B. N. Reinecke, M. A. Arman, L. R. Merte, J. Knudsen, J. Schnadt, J. N. Andersen, and F. Hennies, "The SPECIES beamline at the MAX IV Laboratory: A facility for soft x-ray RIXS and APXPS," J. Synchrotron Radiat. **24**(1), 344–353 (2017).
[44]E. Kokkonen, F. Lopes da Silva, M.-H. Mikkelä, N. Johansson, S.-W. Huang, J.-M. Lee, M. Andersson, A. Bartalesi, B. N. Reinecke, K. Handrup, H. Tarawneh, R. Sankari, J. Knudsen, J. Schnadt, C. Såthe, and S. Urpelainen, "Upgrade of the SPECIES beamline at the MAX IV Laboratory," J. Synchrotron Radiat. **28**, 588 (2021).
[45]G. Halfacree and E. Upton, *Raspberry Pi User Guide*, 1st ed. (Wiley Publishing, 2012).
[46]D. E. Fitzpatrick, M. O'Brien, and S. V. Ley, "A tutored discourse on microcontrollers, single board computers and their applications to monitor and control chemical reactions," React. Chem. Eng. **5**(2), 201–220 (2020).
[47]E. A. Redekop, G. S. Yablonsky, D. Constales, P. A. Ramachandran, C. Pherigo, and J. T. Gleaves, "The Y-procedure methodology for the interpretation of transient kinetic data: Analysis of irreversible adsorption," Chem. Eng. Sci. **66**(24), 6441–6452 (2011).
[48]L.-C. Wang, C. M. Friend, R. Fushimi, and R. J. Madix, "Active site densities, oxygen activation and adsorbed reactive oxygen in alcohol activation on NpAu catalysts," Faraday Discuss. **188**, 57–67 (2016).
[49]C. Reece, E. A. Redekop, S. Karakalos, C. M. Friend, and R. J. Madix, "Crossing the great divide between single-crystal reactivity and actual catalyst selectivity with pressure transients," Nat. Catal. **1**(11), 852–859 (2018).
[50]S. O. Shekhtman, G. S. Yablonsky, J. T. Gleaves, and R. Fushimi, "State defining experiment in chemical kinetics. Primary characterization of catalyst activity in a TAP experiment," Chem. Eng. Sci. **58**(21), 4843–4859 (2003).
[51]J. Schneider, M. Matsuoka, M. Takeuchi, J. Zhang, Y. Horiuchi, M. Anpo, and D. W. Bahnemann, "Understanding $TiO_2$ photocatalysis: Mechanisms and materials," Chem. Rev. **114**(19), 9919–9986 (2014).
[52]M. Nicolas, M. Ndour, O. Ka, B. D'Anna, and C. George, "Photochemistry of atmospheric dust: Ozone decomposition on illuminated titanium dioxide," Environ. Sci. Technol. **43**(19), 7437–7442 (2009).
[53]Y. Chen, S. Tong, J. Wang, C. Peng, M. Ge, X. Xie, and J. Sun, "Effect of titanium dioxide on secondary organic aerosol formation," Environ. Sci. Technol. **52**(20), 11612–11620 (2018).
[54]R. L. Kurtz and V. E. Henrich, "Comparison of Ti 2*p* core-level peaks from $TiO_2$, $Ti_2O_3$, and Ti metal, by XPS," Surf. Sci. Spectra **5**(3), 179–181 (1998).
[55]M. J. Jackman, A. G. Thomas, and C. Muryn, "Photoelectron spectroscopy study of stoichiometric and reduced anatase $TiO_2$(101) surfaces: The effect of subsurface


Published under license by AIP Publishing

defects on water adsorption at near-ambient pressures," J. Phys. Chem. C **119**(24), 13682–13690 (2015).
[56]Y. Wang and M. Makkee, "Fundamental understanding of the Di-air system (an alternative $NO_x$ abatement technology). I: The difference in reductant pre-treatment of ceria," Appl. Catal., B **223**, 125–133 (2018).
[57]T. Suntola and J. Hyvarinen, "Atomic layer epitaxy," Annu. Rev. Mater. Sci. **15**(1), 177–195 (1985).
[58]A. R. Head, S. Chaudhary, G. Olivieri, F. Bournel, J. N. Andersen, F. Rochet, J.-J. Gallet, and J. Schnadt, "Near ambient pressure x-ray photoelectron spectroscopy study of the atomic layer deposition of $TiO_2$ on $RuO_2$(110)," J. Phys. Chem. C **120**(1), 243–251 (2016).
[59]R. Timm, A. R. Head, S. Yngman, J. V. Knutsson, M. Hjort, S. R. McKibbin, A. Troian, O. Persson, S. Urpelainen, J. Knudsen, J. Schnadt, and A. Mikkelsen, "Self-cleaning and surface chemical reactions during hafnium dioxide atomic layer deposition on indium arsenide," Nat. Commun. **9**(1), 1412 (2018).
[60]R. H. Temperton, A. Gibson, and J. N. O'Shea, "*In situ* XPS analysis of the atomic layer deposition of aluminium oxide on titanium dioxide," Phys. Chem. Chem. Phys. **21**(3), 1393–1398 (2019).
[61]G. D'Acunto, A. Troian, E. Kokkonen, F. Rehman, Y.-P. Liu, S. Yngman, Z. Yong, S. R. McKibbin, T. Gallo, E. Lind, J. Schnadt, and R. Timm, "Atomic layer deposition of hafnium oxide on InAs: Insight from time-resolved *in situ* studies," ACS Appl. Electron. Mater. **2**(12), 3915–3922 (2020).


Published under license by AIP Publishing